Draft version December 23, 2020
Typeset using LaTeX default style in AASTeX62

Massive Stellar Triples Leading to Sequential Binary Black-Hole Mergers in the Field

Alejandro Vigna-Gómez,[1] Silvia Toonen,[2] Enrico Ramirez-Ruiz,[3,1] Nathan W.C. Leigh,[4,5] Jeff Riley,[6,7] and Carl-Johan Haster[8,9]

[1] *DARK, Niels Bohr Institute, University of Copenhagen, Jagtvej 128, 2200, Copenhagen, Denmark*
[2] *Institute of Gravitational Wave Astronomy, School of Physics and Astronomy, University of Birmingham, Birmingham, B15 2TT, United Kingdom*
[3] *Department of Astronomy and Astrophysics, University of California, Santa Cruz, CA 95064, USA*
[4] *Departamento de Astronomía, Facultad de Ciencias Físicas y Matemáticas, Universidad de Concepción, Concepción, Chile*
[5] *Department of Astrophysics, American Museum of Natural History, New York, NY 10024, USA*
[6] *Monash Centre for Astrophysics, School of Physics and Astronomy, Monash University, Clayton, Victoria 3800, Australia*
[7] *The ARC Centre of Excellence for Gravitational Wave Discovery – OzGrav*
[8] *LIGO Laboratory, Massachusetts Institute of Technology, 185 Albany St, Cambridge, MA 02139, USA*
[9] *Department of Physics and Kavli Institute for Astrophysics and Space Research, Massachusetts Institute of Technology, 77 Massachusetts Ave, Cambridge, MA 02139, USA*

ABSTRACT

Stellar triples with massive stellar components are common, and can lead to sequential binary black-hole mergers. Here, we outline the evolution towards these sequential mergers, and explore these events in the context of gravitational-wave astronomy and the pair-instability mass gap. We find that binary black-hole mergers in the pair-instability mass gap can be of triple origin and therefore are not exclusively formed in dense dynamical environments. We discuss the sequential merger scenario in the context of the most massive gravitational-wave sources detected to date: GW170729 and GW190521. We propose that the progenitor of GW170729 is a low-metallicity field triple. We support the premise that GW190521 could not have been formed in the field. We conclude that triple stellar evolution is fundamental in the understanding of gravitational-wave sources, and likely, other energetic transients as well.

1. INTRODUCTION

The importance of interactions between massive stars in isolated binaries has become increasingly recognized in the last decades (e.g., Podsiadlowski et al. 1992; Sana et al. 2012). Recent studies indicate that early B and O type stars are almost exclusive part of higher-order configurations, such as triples and quadruple systems (Sana et al. 2014; Moe & Di Stefano 2017). If future surveys confirm this, our understanding of massive stellar evolution will have to include the increased complexity of multiple-body interactions that were previously mostly considered in dense dynamical environments such as nuclear, globular, or open *clusters* (e.g., Sigurdsson & Hernquist 1993; Leigh & Geller 2013).

An alternative to electromagnetic methods to study high-mass stellar multiplicity is gravitational-wave (GW) astronomy, as massive stars are believed to be the progenitors of stellar-mass black holes (BHs). Stellar-mass binary black holes (BBHs) are believed to form predominantly in field binaries (e.g., Belczynski et al. 2002; Neijssel et al. 2019) and clusters (e.g., Portegies Zwart & McMillan 2000; Rodriguez et al. 2019; Leigh et al. 2014). There have been efforts in trying to understand how best to segregate these two different origins, mostly based on eccentricities and spins, yet there is no definitive consensus on the origin of current GW sources (e.g. Abbott et al. 2019).

One candidate signature for cluster origin of a GW is a BH mass in the pair-instability supernova (PISN) *mass gap*[1]. PISNe are initiated by an electron-positron pair-instability which eventually leads to explosive oxygen burning in the core of massive stars (see Langer 2012, and references therein). PISNe do not leave behind remnants and therefore a gap is expected in the mass distribution of BHs for stars with helium core masses in the range of $\approx 64 - 133$ $M_\odot$ (Heger & Woosley 2002). Consequently, isolated binary evolution theory does not predict individual BHs in that

Corresponding author: Alejandro Vigna-Gómez
avignagomez@nbi.ku.dk

[1] In this *Letter* we do not consider the potential mass gap between massive neutron stars and low-mass black holes.

regime (Stevenson et al. 2019; van Son et al. 2020). As multiple BH mergers can populate the mass gap, the discovery of BBH systems with one component lying within the mass gap is considered so far a smoking gun for cluster origin (Rodriguez et al. 2019; Samsing & Hotokezaka 2020). The recent detection of GW190521 (Abbott et al. 2020a), with at least one BH within the mass gap, adds to the conundrum.

Here, we give an overview of which isolated massive stellar triples experience a *sequential merger* of BBHs. We investigate the potential origin of such configurations, put them in the context of GW observations, and focus on the masses and spins of sequential mergers leading to BBHs in the mass gap. We propose that GW170729 is of isolated triple origin, and suggest the mass gap event GW190521 was not formed in the field. Finally, we highlight the importance of massive stellar triples in a broader astronomical context.

2. METHOD

Here, we outline our main assumptions for the key physics of the formation of a sequential merger starting at the zero-age main sequence. We consider isolated hierarchical triple systems, composed of an inner binary with masses $M_1 \geq M_2$ and an outer companion of mass M_3. In the sequential mergers that we consider here the inner BBH merges first, and afterwards the remnant merges with the outer BH. We adopt circular coplanar prograde orbits, as supported by observations of compact triples (Tokovinin 2017). For circular coplanar prograde orbits we do not expect Lidov-Kozai cycles and neglect other three-body dynamical effects (see, e.g., Naoz 2016, for a review).

The triple must remain dynamically stable from the zero-age main sequence until the inner BBH merger, which holds if (Mardling & Aarseth 2001):

$$\frac{a_{\rm out}}{a_{\rm in}} \geq \left(\frac{a_{\rm out}}{a_{\rm in}}\right)_{\rm crit} \equiv \frac{2.8}{1-e_{\rm out}}\left[\frac{(1+q_{\rm out})(1+e_{\rm out})}{\sqrt{1-e_{\rm out}}}\right]^{2/5}, \tag{1}$$

where a is the semi-major axis, e is the eccentricity and q is the mass ratio (the inner and outer orbits are specified by the *in* and *out* subscripts). The outer mass ratio is $q_{\rm out} \equiv M_3/(M_1+M_2)$.

We use the synthetic BBH population from Riley et al. (2020) based on isolated binary evolution to investigate the orbital properties of the inner binary (Appendix for further details). The models include mass loss, mass transfer, supernovae and chemically homogeneous evolution (CHE). In Figure 1 we present their intrinsic mass distribution of merging BBHs. We focus on low-metallicity stars ($Z \lesssim 10^{-3}$) in order to neglect mass loss, spin-down and orbital changes due to stellar winds.

As each star of the triple evolves, it will eventually become a BH with mass $M_{\rm BH,i}$ (with $i = 1,2,3$), for which we assume the following. BHs have a minimum mass of $M_{\rm BH,min} = 2.5$ M$_\odot$. There is a mass gap between $43 \lesssim M_{\rm gap}/{\rm M}_\odot \lesssim 124$ (du Buisson et al. 2020) due to PISN . The exact lower limit of the mass gap is uncertain, and might be as high as $M_{\rm BH} \approx 50$ M$_\odot$ (for an overview see Stevenson et al. 2019, and references therein). Furthermore, we assume that stars with carbon-oxygen core masses above 11 M$_\odot$ experience complete fallback (Fryer et al. 2012) and negligible neutrino mass loss (Müller et al. 2016), likely suppressing BH natal kicks. All BHs are born as slow rotators (Fuller & Ma 2019).

During the inner BBH merger, mass is lost by radiation from the center of mass of the merging BBH. This leads to a GW Blaauw-kick similar to that in spherically symmetric supernovae (Blaauw 1961). The fraction of radiated mass with respect to the mass of the merging BBH ($f_{\rm rad}$) depends on the masses and spins of the system (Appendix). This modifies the orbit of the tertiary:

$$\frac{a_{\rm out,post}}{a_{\rm out,pre}} = \left[2 - \frac{M_{\rm BH,1}+M_{\rm BH,2}+M_{\rm BH,3}}{M_{\rm BBH,in}+M_{\rm BH,3}}\right]^{-1}, \tag{2}$$

and

$$e_{\rm out,post} = \frac{f_{\rm rad}(M_{\rm BH,1}+M_{\rm BH,2})}{M_{\rm BBH,in}+M_{\rm BH,3}}, \tag{3}$$

where $M_{\rm BBH,in} \approx (1-f_{\rm rad})(M_{\rm BH,1}+M_{\rm BH,2})$. For non-spinning BBHs and assuming $e_{\rm out,pre} \approx 0$, $f_{\rm rad} \approx 0.05$, $e_{\rm out,post} \approx 0.05$ and $a_{\rm out,post} \approx 1.06 \times a_{\rm out,pre}$. Furthermore, conservation of momentum gives rise to a recoil kick, which has a magnitude of zero when $q_{\rm BBH,in} \approx 0$ or $q_{\rm BBH,in} \approx 1$ and can be as high as $v_{\rm recoil} \lesssim 175$ km s^{-1} for

$q_{\rm BBH,in} \approx 0.36$ (González et al. 2007). As our synthetic population favors $q_{\rm BBH,in} \gtrsim 0.9$ (Figures 1 and 2), the magnitude of the recoil kick should be small and we ignore it. The radiated mass fraction is maximal ($f_{\rm rad,max} \approx 0.12$) when we consider a merger from an equal-mass maximally-spinning BBH that is aligned with the orbital spin. This constrains the post-merger eccentricity and separation to $e_{\rm out} \lesssim 0.14$ and $a_{\rm out,post} \lesssim 1.16 \times a_{\rm out,pre}$ respectively. The systems we consider here can therefore not be unbound during the inner BBH merger.

We assume the outer orbit is almost circular at all times. In this case the GW inspiral time can be approximated with (Peters 1964):

$$T_c \approx \frac{5}{256} \frac{c^5 a_{\rm out}^4}{G^3 M_{\rm BBH,in} M_{\rm BH,3} (M_{\rm BBH,in} + M_{\rm BH,3})}. \tag{4}$$

We estimate the effective spin of the sequential merger as

$$\chi_{\rm eff} = \frac{(M_{\rm BBH,in}\vec{\chi}_{\rm BBH,in} + M_{\rm BH,3}\vec{\chi}_{\rm BH,3}) \cdot \hat{L}_{\rm N}}{M_{\rm BBH,in} + M_{\rm BH,3}} = \frac{|\vec{\chi}_{\rm BBH,in}|}{1 + M_{\rm BH,3}/M_{\rm BBH,in}}, \tag{5}$$

where $\vec{\chi}$ is the dimensionless component spin of the BH and $\hat{L}_{\rm N}$ is the unit vector parallel to the system's orbital angular momentum. For a merger of an equal mass inner non-rotating BBH, the remnant has a spin magnitude of $|\vec{\chi}_{\rm BBH,in}| \approx 0.68$ (Boyle et al. 2008).

3. RESULTS

3.1. *BH mass parameter-space for sequential mergers*

In Figure 1 we display the possible mass combinations of inner BBHs and outer BHs for sequential mergers. We denote the (PISN) mass gap in grey. Assuming single stellar evolution for the tertiary, the mass gap for the outer BH is between $M_{\rm gap,min} = 43\ {\rm M}_\odot \lesssim M_{\rm BH,3} \lesssim M_{\rm gap,max} = 124\ {\rm M}_\odot$. The corresponding mass gap for the inner BBH is shifted to $2 \times M_{\rm gap,min} = 86\ {\rm M}_\odot \lesssim M_{\rm BBH,in} \lesssim M_{\rm gap,max} + M_{\rm BH,min} = 126.5\ {\rm M}_\odot$.

In Figure 1 we classify four regions of interest: red, blue, yellow and green. The red region comprises $M_{\rm BBH,in} < M_{\rm BH,3}$, where the outer (more massive) BH collapses before the other BHs form, based on stellar evolution timescales. The blue region comprises $M_{\rm BH,3} < M_{\rm BBH,in}$ with $M_{\rm BBH,in} \lesssim 86\ {\rm M}_\odot$ and $M_{\rm BH,3} \lesssim 43\ {\rm M}_\odot$. Most GW sources detected to date are in the red and blue region below the mass gap (Abbott et al. 2019). The yellow region comprises $M_{\rm BBH,in} \gtrsim 126.5\ {\rm M}_\odot$ with $M_{\rm BBH,in} \gg M_{\rm BH,3}$ and $M_{\rm BH,3} \lesssim {\rm M}_{\rm gap,min} \approx 43\ {\rm M}_\odot$. Finally, the green region comprises $M_{\rm BBH,in} > M_{\rm BH,3}$ with $M_{\rm BBH,in} \gtrsim 126.5\ {\rm M}_\odot$ and $M_{\rm BH,3} \gtrsim 124\ {\rm M}_\odot$. The rare sequential mergers from the green region will have masses above the mass gap and are not discussed any further.

3.2. *Types of Triples*

For the evolution of the stars, we consider *standard evolving* and *compact* constituent stars. Standard evolving stars rotate slowly, develop a composition gradient, and can expand up to thousands of solar radii during their evolution (e.g., Podsiadlowski et al. 1992). This expansion is avoided by stars in metal-free (Pop III) environments (Marigo et al. 2001), in certain mass-metallicity regimes (Shenar et al. 2020) or that rotate rapidly such that rotational mixing is induced (Maeder 1987), i.e. CHE. The orbits of CHE binaries can therefore remain more compact throughout their evolution to BBH formation as compared to binaries with standard evolving stars (Marchant et al. 2016; de Mink & Mandel 2016; Riley et al. 2020). This is favorable for the sequential merger channel in order for the triple to remain dynamically stable as well as compact enough to lead to two mergers within a Hubble time (Equation 1 & 4). We therefore consider four distinct types of stellar triples (illustrated in Figure 3): 1) an inner binary with compact stars and an outer standard evolving star, 2) all compact stars, 3) at least one standard evolving star in the inner binary with an outer standard evolving companion, and, 4) at least one standard evolving star in the inner binary with an outer compact star.

3.3. *Populating the (PISN) mass gap*

From the full BH mass range (Figure 1) we extract sequential mergers with total mass within the mass gap, classify them in sub-regions (Figure 2), discuss their evolutionary pathways (Figure 3), and present their demographics (Figure 4 and Table 1).

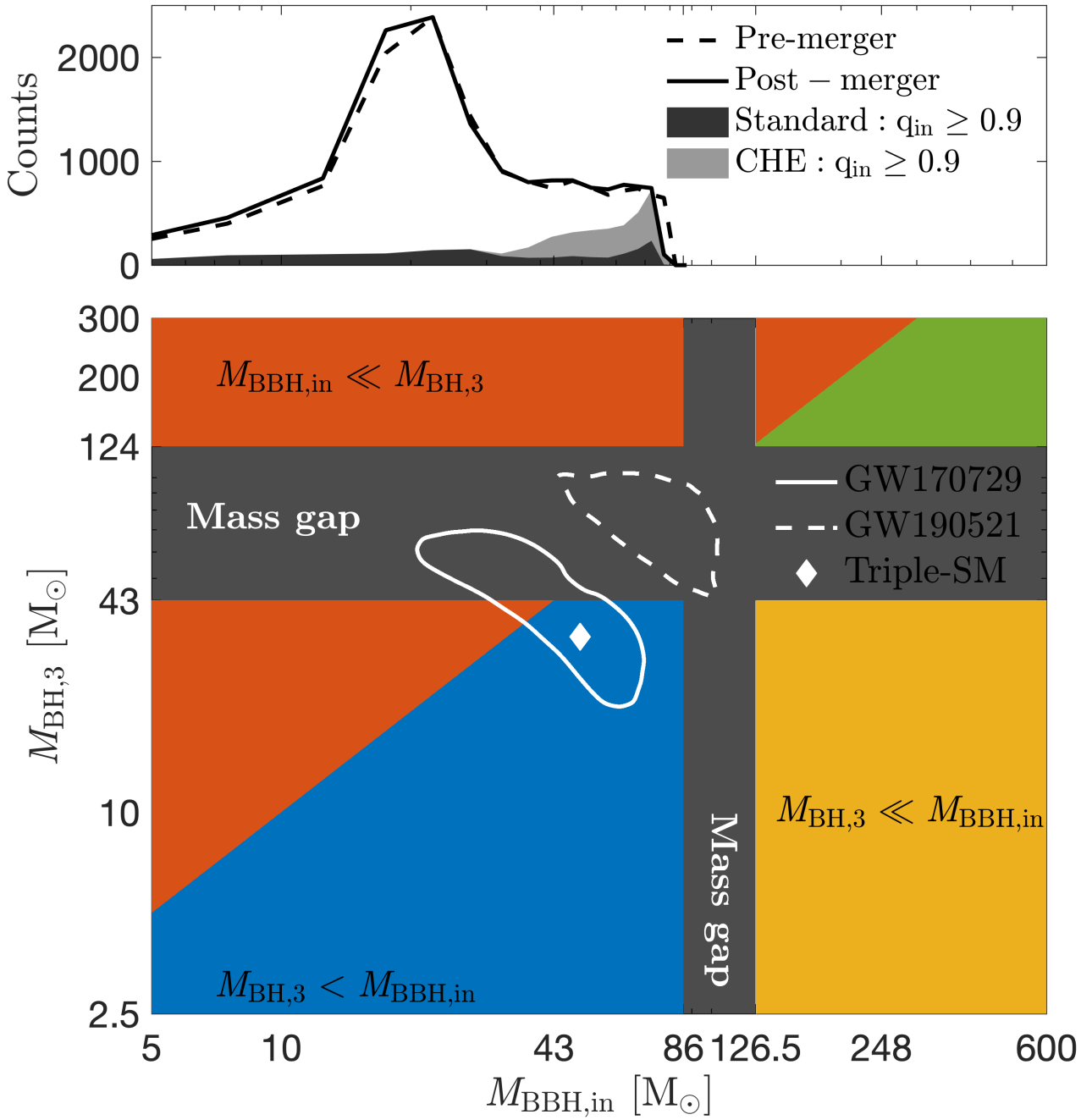

Figure 1. Overview of mass combinations for isolated triples leading to sequential mergers. Top: Mass distribution of merging BBHs for the inner binary based on isolated binary evolution calculations (Riley et al. 2020). The solid (dashed) black line is the mass distribution after (before) the inner BBH merger. Shaded regions highlight standard evolving (dark grey) and CHE (light grey) systems with $q_{in} \geq 0.9$. Bottom: The area colored grey is the approximate mass gap region where BHs from isolated binary origin are not expected to form due to PISNe (Section 3.1). The coloured regions are described in Section 3.1 and examples are illustrated in Figure 3. The diamond is an example of a sequential merger (Triple-SM) as discussed in Section 3.4. White solid and dashed contours are the 90% confidence intervals for GW170729 (Chatziioannou et al. 2019) and GW190521 (Abbott et al. 2020a), respectively.

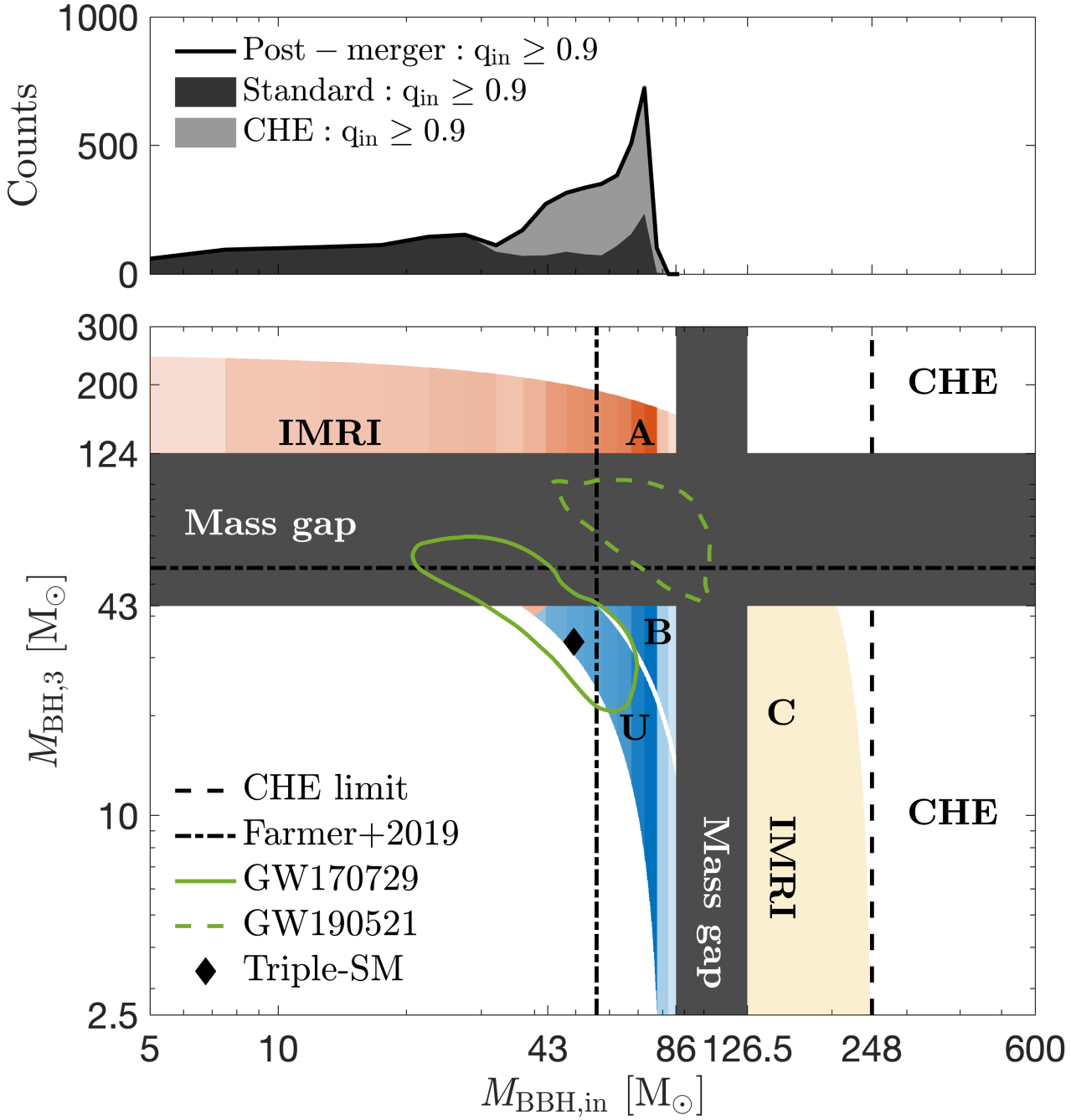

Figure 2. Overview of mass combinations for isolated triples leading to sequential mergers with total mass in the (PISN) mass gap. Similar to Figure 1 but only accounting for sequential mergers that have final total mass within the mass gap. For the mass of the inner BBH the intensity of the color reflects the bin weight from the mass histogram (top panel). We explore mass gap sequential mergers in the red (A), blue (B) and yellow (C) regions (Section 3.3 for full description). Blue sub-region B only includes sources well within the mass gap with total mass $(M_{\rm BBH,in} + M_{\rm BH,3})/{\rm M}_\odot > 100$. To incorporate model uncertainties, we lower the threshold to between $80 \leq (M_{\rm BBH,in} + M_{\rm BH,3})/{\rm M}_\odot \leq 100$ (Stevenson et al. 2019) for region U. The black dash-dotted line at $M_{\rm BBH,in} = 56$ M$_\odot$ corresponds to the maximum single BH mass according to Farmer et al. (2019). The area encompassed to the right of this limit and the left of the mass gap is not populated by single stellar evolution. The black dashed line corresponds to $2 \times M_{\rm gap,max} \approx 248$ M$_\odot$, the minimum combined mass for CHE BBHs above the mass gap (du Buisson et al. 2020). Intermediate mass-ratio inspirals (IMRIs) can be in the red and yellow regions. See Figure 1 for further explanations and Figure 3 for an illustration of the evolution of these systems.

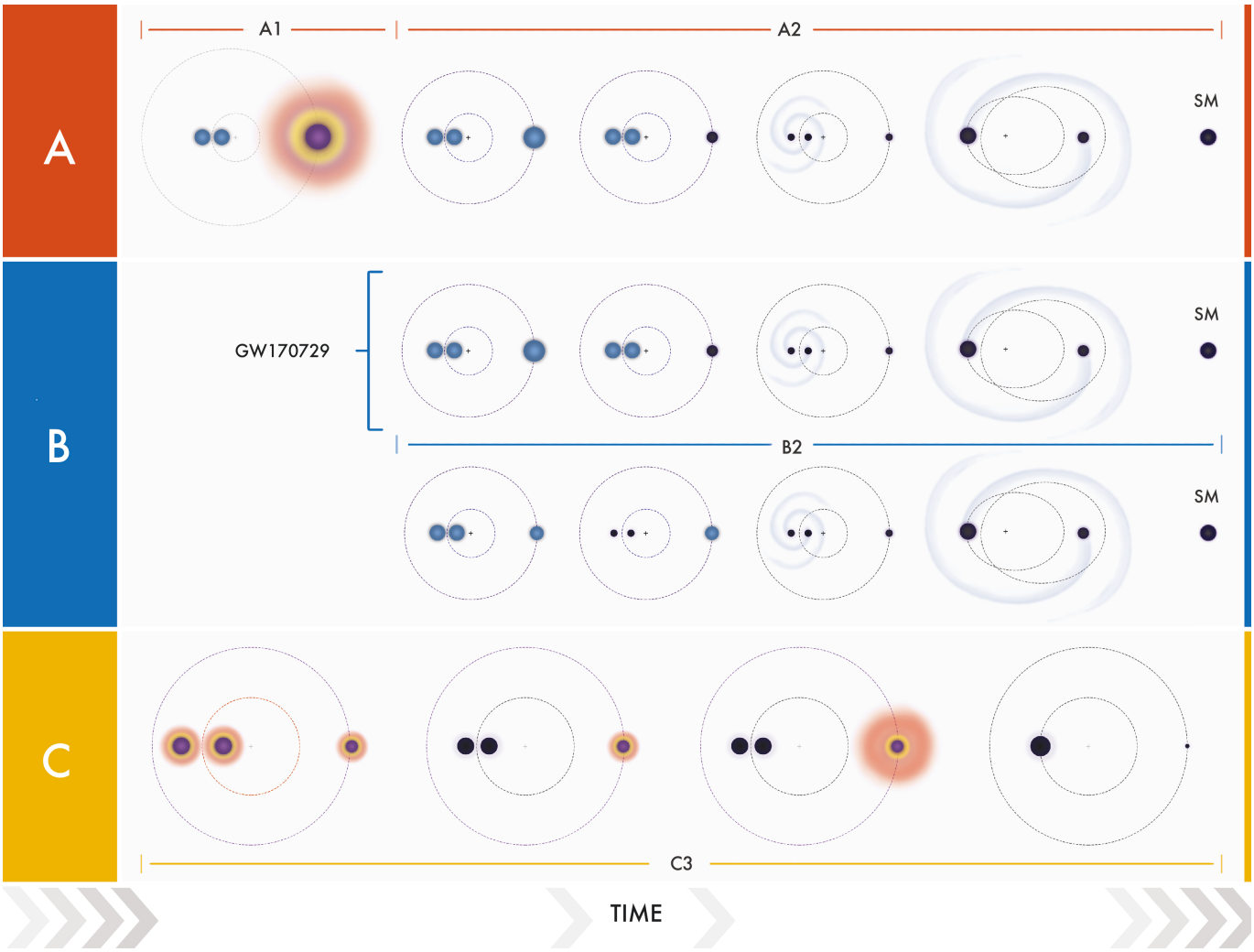

Figure 3. Time evolution of triple stellar systems. We illustrate compact stars in blue, standard evolving stars with red envelopes, BHs in black and merging BBHs with a surrounding swirl. BHs formed as sequential mergers are labeled *SM*. Architectures are described in Sections 3.1 and 3.2, and discussed in Section 3.3. Top: Red sub-region A, where the tertiary is the most massive star in the system and forms the first BH in this triple. The inner binary needs to be constituted of compact stars and the tertiary can be either standard evolving or a compact star (Triple Types 1 and 2 respectively). Middle: Blue sub-region B, where all stars have similar masses. These triples can only lead to sequential mergers if all stars are compact (Triple Type 2). We suggest GW170729 experienced this evolution. Bottom: Yellow sub-region C, where the tertiary is of significantly lower mass than either of the inner binary stars. We find that this configuration (Triple Type 3) does not lead to sequential mergers and is only presented for completion. Credit: T. Rebagliato.

3.3.1. *Red sub-region A*

The predicted properties of systems in red sub-region A are $M_{\rm BBH,in} \ll {\rm M}_{\rm gap,max} \leq M_{\rm BH,3}$ and $0.1 \lesssim \chi_{\rm eff} \lesssim 0.27$. The evolution of an example system is illustrated in the top panel of Figure 3. Consider a CHE inner binary (Triple Type 1 or 2) with $M_1 \approx M_2 \approx 40$ M$_\odot$, $R_1 \approx R_2 \approx 6$ R$_\odot$ and $a_{\rm in} \gtrsim 18$ R$_\odot$. All stars in this triple will experience complete fallback, which effectively leave the inner and outer orbits unchanged (Section 2). Assuming the outer star collapses to a BH with mass $M_{\rm BH,3} \approx 140$ M$_\odot$, then $a_{\rm out} \gtrsim (a_{\rm out}/a_{\rm in})|_{\rm crit} \times a_{\rm in} \approx 4.2 \times (18$ R$_\odot) \approx 76$ R$_\odot$ in order for the triple to be stable (Equation 1 and Figure 4). If the separation after the inner BBH merges is less than $a_{\rm out,max} \lesssim 122$ R$_\odot$, then the sequential merger can occur within a Hubble time (Equation 4). The critical ratio of $a_{\rm out}/a_{\rm in}$ to maintain stability and the maximum orbital separation to achieve a merger within a Hubble time depend on the mass combinations of the triple, and vary within a factor of a few for the combinations of interest here (Figure 4).

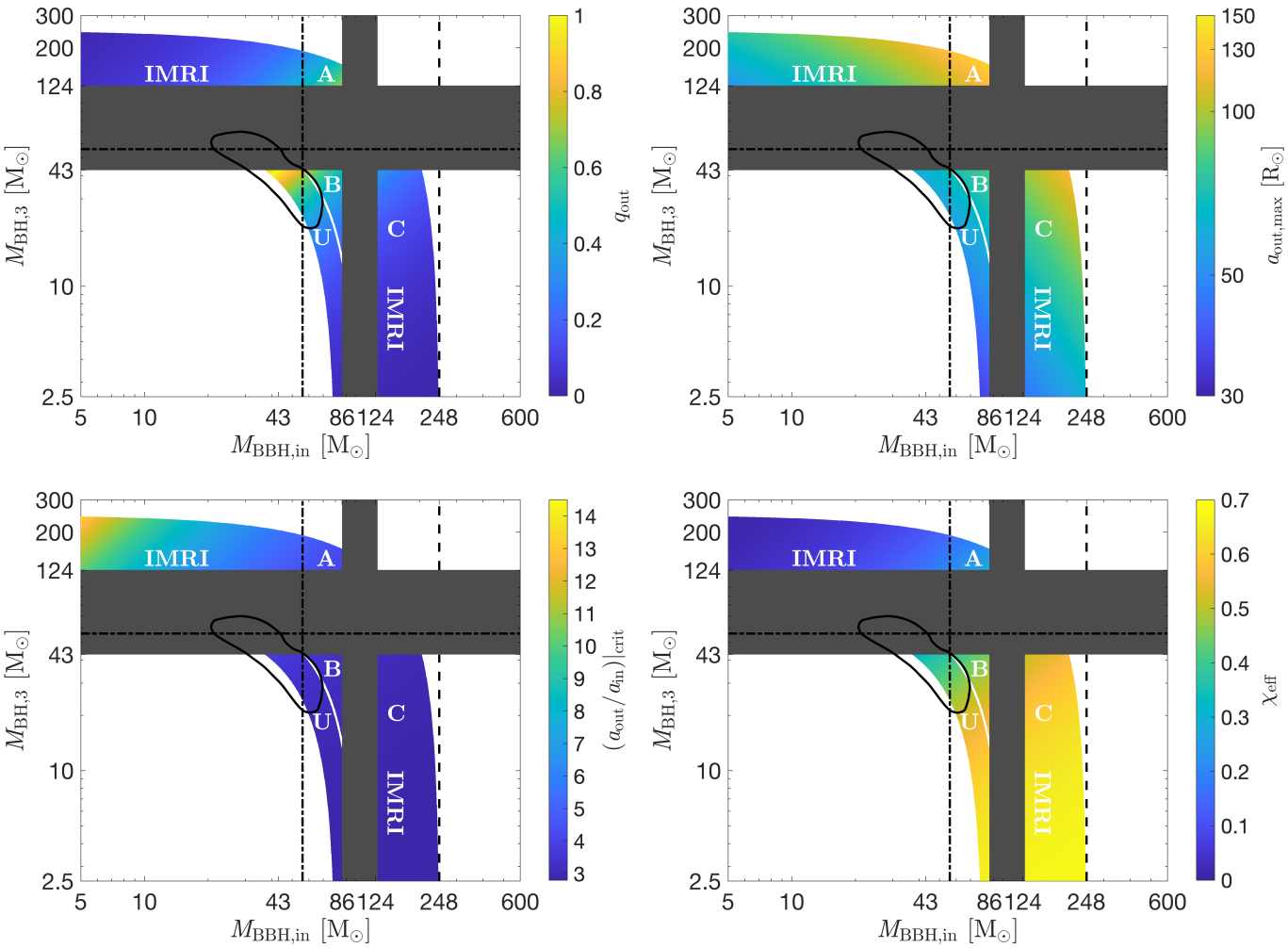

Figure 4. Overview of mass combinations for isolated triples leading to sequential mergers with total mass in the (PISN) mass gap (see caption in Figure 1 and 2 for additional details). The color in each panel denotes a different physical property. 90% confidence intervals for GW170729 (Chatziioannou et al. 2019) shown as a solid black line. Top left: outer mass ratio ($q_{\rm out}$) for the sequential merger. Top right: maximum separation in which a circular binary with component masses $M_{\rm BBH,in}$ and $M_{\rm BH,3}$ can merger within the age of the Universe due to GW emission. Bottom left: minimum ratio of outer and inner orbital separation for dynamical stability assuming a circular coplanar prograde orbit. Bottom right: effective dimensionless spin ($\chi_{\rm eff}$) of the sequential merger, assuming coplanarity in the inner and outer orbit. Note that $\chi_{\rm eff} > 0$ and $\chi_{\rm eff} \approx 0.4$ for LVC-like sources (around sub-region B).

If the outer star was initially a standard evolving star (Triple Types 1 and 3) it might initiate a mass transfer phase onto the inner binary early in the evolution of the system (step A1 in Figure 3). This could occur if the radius of a standard evolving star exceeds the Roche lobe radius, i.e. $R_3 \gtrsim 0.43 \times a_{\rm in}$ for $q_{\rm out} \approx 140/80$. Assuming the stellar radii approach $\sim 100 - 1000\ R_\odot$ at maximum (Podsiadlowski et al. 1992; Riley et al. 2020), tertiary driven mass transfer occurs for outer orbits up to several $\sim 100 - 1000\ R_\odot$.

During this mass transfer phase, where the tertiary donor is significantly heavier than the inner binary, the outer orbit likely shrinks (based on angular momentum considerations) and the hydrogen envelope is stripped off the outer star. If the inner binary avoids a merger during this stage (see, e.g., Leigh et al. 2020), at the end of the mass transfer phase, the tertiary is a stripped helium star reminiscent of the compact outer star considered in Triple Type 2.

In this section so far we have considered inner binaries comprising of CHE stars which remain close to each other throughout their evolution to BBHs. However, for standard evolving inner binaries (Triple Types 3 and 4), the orbital separation can change drastically between the zero-age main sequence and BBH formation due to mass and angular momentum exchanges during mass transfer episodes. From our synthetic population, the orbits of standard evolving

Table 1. Summary of expected demographics of different types of sequential mergers. This Table summarizes the results from Section 3 and all Figures. For each quantity of interest we present the minimum and maximum values in between square brackets. We have subjectively provided a ranking for most likely (1) to less likely (5) scenario to form a sequential merger, based on the inner BBH mass distribution, the condition for triple stability and the sequential merger time. Masses and separations are in solar units.

Region	A-IMRI	A	U	B	C-IMRI
Rank	4	2	1	3	5
Region	Red	Red	Blue	Blue	Yellow
Triple type	1	1 & 2	1 & 2	1 & 2	3
Mass gap $M_{\rm BBH,in}$	No	Yes	Uncertain	Yes	No
$M_{\rm BH,3}$	[124,243]	[124,205]	[2.5,43]	[14,43]	[2.5,43]
$M_{\rm BBH,in}$	[5,43]	[43,86]	[37,86]	[57,86]	[126.5,245.5]
$M_{\rm BH,3}+M_{\rm BBH,in}$	[129,248]	[167,248]	[80,100]	[100,129]	[129,248]
$q_{\rm out}$	[0,0.1]	[0.1,0.69]	[0,1]	[0.16,0.74]	[0,0.1]
$a_{\rm out}$	[52,120]	[97,135]	[35,69]	[57,82]	[45,120]
$\chi_{\rm eff}$	[0,0.1]	[0.1,0.27]	[0.4,0.68]	[0.38,0.58]	[0.5,0.68]
$(a_{\rm out}/a_{\rm in})\vert_{\rm crit}$	[4.8,13.3]	[4.0,5.7]	[2.8,3.8]	[3.0,3.3]	[2.8,3.1]

binaries can remain as small as $a_{\rm in} \approx 70$ R$_\odot$ throughout their evolution, but for most systems their orbits expand to hundreds or thousands of solar radii (see, e.g. Leigh et al. 2020). Assuming the optimistic case of a standard evolving inner binary with $a_{\rm in} \approx 70$ R$_\odot$ maximally, the outer separation must be $a_{\rm out} \geq 2.8 \times (70$ R$_\odot) \approx 196$ R$_\odot$ in order for the triple to be stable throughout its full evolution. Such an orbit does not merge by GW emission alone in a Hubble time (Figure 4). We conclude that in red sub-region A only triples with inner compact binaries can lead to sequential mergers within a Hubble time.

3.3.2. *Blue sub-region B*

The predicted properties of systems in blue sub-region B are $M_{\rm BBH,in}/2 \approx M_{\rm BH,out} \leq$ M$_{\rm gap,min}$ and $0.38 \lesssim \chi_{\rm eff} \lesssim 0.58$. The evolution of an example system is illustrated in the middle panel of Figure 3. Furthermore, the synthetic population suggests $M_{\rm BH,1} \approx M_{\rm BH,2}$ in this region; with similar BH masses the evolutionary timescales for all component stars are similar as well. Consider a triple with $M_1 \approx M_2 \approx M_3 \approx 40$ M$_\odot$. We again assume a CHE inner binary (Triple Type 1 or 2) with $R_1 \approx R_2 \approx 6$ R$_\odot$ and $a_{\rm in} \gtrsim 18$ R$_\odot$. This triple is dynamically stable if $a_{\rm out} \gtrsim 3.3 \times (18$ R$_\odot) \approx 60$ R$_\odot$. The outer separation must be $a_{\rm max} \lesssim 76$ R$_\odot$ for the sequential merger to occur within a Hubble time due to GW emission. Hence the small possible range for outer separations between $60 \lesssim a_{\rm out}/$R$_\odot \lesssim 76$ constraints the feasibility and frequency of this sub-channel. Pop III BBH progenitors with initial masses $M_1 \gtrsim 40$ M$_\odot$ and $q \approx 1$ have initial separations $a_{\rm in} \gtrsim 20$ R$_\odot$ (Inayoshi et al. 2017), which lead to slightly more stringent constraints than for CHE binaries.

If the tertiary was a standard evolving star (Triple Types 1 and 3), it could initiate a mass transfer episode onto the inner binary. Due to the mass ratio, we expect this mass transfer to proceed in a stable manner. Furthermore, we expect the outer orbit to widen typically due to angular momentum evolution, which makes the sequential merger less likely to occur within a Hubble time (see, e.g., Belczynski et al. 2002, for an overview in the context of BBH progenitors). In summary, in the blue sub-region B only triple compact binaries in a fine tuned configuration can lead to sequential mergers within a Hubble time.

3.3.3. *Yellow sub-region C*

The masses of systems in yellow sub-region C are $M_{\rm BH,3} \ll$ M$_{\rm gap,max} \leq M_{\rm BBH,in}$. The evolution of an example system is illustrated in the bottom panel of Figure 3. Even though our synthetic binary population does not predict any inner BBHs in this region (Appendix), BBHs above the mass gap have been suggested for both compact (Marchant et al. 2016; du Buisson et al. 2020) and standard evolving (Mangiagli et al. 2019) binaries. Regarding the former, as inner binaries experiencing CHE (Triple Types 1 or 2) are expected to have mass ratios $q_{\rm in} \approx 1$ and $M_{\rm BBH,in} \gtrsim 2 \times M_{\rm gap,max} \approx 248$ M$_\odot$, these systems can only bring about sequential mergers with a total mass above the mass gap. Regarding the latter, the case of hypothetical standard evolving binaries is also not promising for sequential mergers. If mass transfer would take place from the lower-mass tertiary companion to the heavier-mass inner binary, it would likely be stable and

widen the outer orbit. This would increase the GW inspiral time for the outer orbit. Therefore, we do not consider sequential mergers from sub-region C to be common.

3.4. *GW170729 as a sequential merger*

GW170729, with a reported chirp mass $\mathcal{M} = (M_1 M_2)^{3/5}/(M_1 + M_2)^{1/5} = 35.4^{+6.5}_{-4.8}$ M$_\odot$, post-merger remnant BH mass of $79.5^{+14.7}_{-10.2}$ M$_\odot$, $\chi_{\rm eff} = 0.37^{+21}_{-25}$ and redshift $z = 0.49^{+0.19}_{-0.21}$ (Abbott et al. 2019), can be marginally considered in the mass gap (Figures 1, 2, and 4). While Rodriguez et al. (2019) associates GW170729 with cluster origin, Kimball et al. (2020) claims a standard stellar evolution origin. Here we propose that the heavier BH of GW170729, with an inferred mass of $50.2^{+16.2}_{-10.2}$ M$_\odot$, is the remnant of an inner BBH from a sequential merger.

The scenario we suggest is the following. We consider a CHE system (Triple Type 3) at metallicity $Z = 10^{-4}$ with an inner over-contact binary of $M_1 = M_2 = 29$ M$_\odot$, $R_1 = R_2 \approx 4.8$ R$_\odot$, $a_{\rm in} \approx 10.5$ R$_\odot$ and a tertiary companion with $M_3 = 33.5$ M$_\odot$, $a_{\rm out} = 43.5$ R$_\odot$ and $e_{\rm out} = 0$. This satisfies the stability condition for the triple as $a_{\rm out} > 3.4 \times (10.5\ {\rm R}_\odot) \approx 35$ R$_\odot$ (Figure 4). At that time, the outer orbit has a relative speed of $\sqrt{G(M_1 + M_2 + M_3)/a_{\rm out}} \approx 600$ km s^{-1}. All stars in this triple will experience complete fallback and negligible stellar winds, which effectively leave the inner and outer orbits unchanged. The only mass change during BH formation comes from the relation between baryonic and gravitational mass (Fryer et al. 2012). The first star to collapse to a ≈ 30.2 M$_\odot$ BH is the tertiary at around 6 Myr. Subsequently the inner binary evolves into a $\approx 26 + 26$ M$_\odot$ BBH at around 7 Myr. Afterwards evolution is purely driven by GW radiation. It takes the inner binary $\sim$50 Myr to merge and form a single BH with $M_{\rm BBH,in} \approx (1 - f_{\rm rad})(M_{\rm BH,1} + M_{\rm BH,2}) \approx 49.5$ M$_\odot$, spin $|\vec{\chi}_{\rm BBH,in}| = 0.68$ (Boyle et al. 2008), separation $a_{\rm out} \approx 45$ R$_\odot$ (Equation 2) and $e_{\rm out} \approx 0$ (Equation 3). After ~ 5.1 Gyr (Equation 4) the second merger takes place. This sequential merger has a chirp mass of ≈ 33.5 M$_\odot$, $\chi_{\rm eff} \approx 0.4$ (Figure 4) and $z \approx 0.49$ (Appendix for redshift calculation and details on the evolution) and is shown in Figures 1 and 2 as a diamond (Triple-SM).

3.5. *GW190521: a BBH in the mass gap*

The inferred total mass of GW190521 is within the mass gap with BH component masses of 85^{+21}_{-14} M$_\odot$ and 66^{+17}_{-18} M$_\odot$ (Abbott et al. 2020a,b). The heavier BH of GW190521 has a mass greater than 60 M$_\odot$ (Fishbach & Holz 2020) and therefore can not be easily associated to isolated binaries (Section 4.3). While uncertainties in the inferred component masses make it tempting to associate GW190521 with a triple origin the inferred spins suggest otherwise. The high individual spins ($|\vec{\chi}_{1,2}| > 0.69$) and low effective spin ($\chi_{\rm eff} \approx 0$) imply that BH spins are not aligned with the orbit (Equation 5). We conclude that GW190521 is inconsistent with our predictions of sequential mergers.

4. DISCUSSION

4.1. *Main caveats to our method*

The main caveats of the scheme presented in this *Letter* are the natal properties of BHs and the assumed orbital distributions (Section 4.2). The remnant masses, birth spins and natal kicks of BHs remain an open question in astrophysics. The assumption of low (Pop II and III) metallicity and complete fallback make mass loss and natal kicks negligible (Fryer et al. 2012; Müller et al. 2016). This is favorable for sequential mergers because any potential widening of the inner orbit can trigger a dynamical instability of the triple and increase the GW inspiral time. However, some models of CHE binaries predict Wolf-Rayet mass loss is non-negligible (e.g., Marchant et al. 2016). Complete fallback is less likely for BH progenitors with carbon-oxygen masses $\lesssim 11$ M$_\odot$ (Fryer et al. 2012), some of which are associated to GW sources (see, e.g., GW170608 from Abbott et al. 2019).

Natal kicks could tilt the orbital spins, change eccentricities and induce inclinations, modifying the evolution from the moment the first BH is born. In some cases, the direction and magnitude of the kick could decrease the inner BBH merger timescale; in others, it could ionize the triple before the sequential merger (other effects discussed in Section 4.2). The extreme case of natal kicks with velocities $\gtrsim 100$ km s^{-1} could even disrupt the system at BH formation.

The spin transition from star to BH is also quite uncertain. Recent studies suggest that angular momentum transport (Fuller & Ma 2019) and accretion feedback (Batta & Ramirez-Ruiz 2019) disfavor maximally spinning BHs. While most BHs are probably born with low spins, CHE can lead to moderate and even high spins (Fuller & Ma 2019). Spin alignment with the orbital angular momentum vector (e.g., CHE binaries) prevents a GW recoil kick even for maximally spinning BHs. Moderate and high misaligned spins can lead to GW recoil kicks of tens or hundreds of km s^{-1} (Lousto et al. 2010). These kicks would not necessarily disrupt our systems (e.g., Section 3.4).

We assume no rotation at birth in order to establish lower limits on effective spins, but remain agnostic on what should a realistic natal BH kick and spin distribution be.

4.2. *Stellar triples: birth distributions and orbital evolution*

The expected rate of sequential mergers depends on the abundance of massive triples and their architectures. Even though these are unconstrained at low metallicities, observations in the Local Group indicate that for O-type stars between $16 \leq M/\mathrm{M}_\odot \leq 40$, the triple multiplicity fraction is ≈ 0.35 (Moe & Di Stefano 2017). Multiplicity in massive stars affects the evolutionary outcomes of field systems, and isolated binary, triple and quadruple evolution jointly contribute to, e.g., the double compact object merger rate.

Close observed systems ($P_{\rm orb} \lesssim 1$ AU) are preferably circular (Sana et al. 2012; Moe & Di Stefano 2017). Observations of tight ($\lesssim 50$ AU) low and intermediate mass ($\lesssim 4$ $\mathrm{M}_\odot$) triples show a strong tendency towards orbital alignment ($\lesssim 36^\circ$) and are therefore likely to avoid Lidoz-Kozai cycles (Tokovinin 2017). However, the orbital distributions of massive stellar triples are yet unknown. Diverging from our simplified assumption of circular coplanar prograde orbits might abruptly modify the evolution of the BH triple due to three-body dynamics. This would induce high(er) eccentricities (Naoz 2016) in the inner binary that may lead to exchanges of mass, mergers (Iben & Tutukov 1999; Moe & Di Stefano 2017) and disruptions (e.g., He & Petrovich 2018). Additionally, mass transfer initiated from the tertiary could have the gaseous envelope change the characteristics of the inner binaries with respect to our adopted synthetic population (de Vries et al. 2014). It may even provoke a merger of the inner binary and provide an electromagnetic counterpart (Leigh et al. 2020). In general, mergers between the two stars of a triple can lead to different systems than the ones expected from pristine binaries (e.g., Podsiadlowski et al. 1992; Vigna-Gómez et al. 2019). It is therefore likely that triples play a non-negligible role in massive stellar evolution.

Eccentricity of the outer orbit is an additional caveat. While the GW coalescence timescale is significantly shorter for eccentric binaries (Peters 1964), the minimum ratio of $a_{\rm out}/a_{\rm in}$ to guarantee dynamical stability is larger for more eccentric systems (Mardling & Aarseth 2001). Both of these directly affect the number of sequential mergers.

Future observations of massive stars will shed light on the orbital birth distributions of triples and will help constrain the validity of our assumptions, the rate of sequential mergers and constrains on their observables.

4.3. *Uncertainties in the (PISN) mass gap*

The exact location and existence of the mass gap is an open question(see, e.g., Belczynski 2020, and references therein). Any model uncertainties on the limits of the mass gap directly propagate to the predicted BBH mass distribution of sequential mergers. Metal-free (Pop III) stars, which can be compact and are believed to lead to more massive BH progenitors, have been suggested to shift the edge of the mass gap (e.g., Farrell et al. 2020; Tanikawa et al. 2020). Helium stellar models predict that the location of the lower edge of the mass gap is robust against variations in (Pop II) metallicity, treatment of rotational mixing and wind mass loss but sensitive to nuclear reaction rates giving $40 \lesssim M_{\rm gap,min}/\mathrm{M}_\odot \lesssim 56$ (Farmer et al. 2019). Variation on the $^{12}\mathrm{C}(\alpha,\gamma)^{16}\mathrm{O}$ rate could shift the limit to $M_{\rm gap,min}/\mathrm{M}_\odot \lesssim 56-90$ (Farmer et al. 2020) and even make the mass-gap disappear (Costa et al. 2020). Different supernova prescriptions lead to an uncertainty between $40 \lesssim M_{\rm gap,min}/\mathrm{M}_\odot \lesssim 50$ (Stevenson et al. 2019). Mass transfer in binaries does not significantly affect the location of the mass gap (van Son et al. 2020). GW sources are an exciting prospect to study the mass gap, with the caveat that they must be first segregated into field or cluster origin.

4.4. *Multiple BH mergers*

Mass gap mergers are usually associated with multiple BH mergers in clusters (e.g. GW190521 as discussed in Abbott et al. 2020b, and references therein). Such mergers are expected to occur readily when central densities are high (Samsing & Hotokezaka 2020). Multiple BH mergers lead to effective spins between $-0.5 \lesssim \chi_{\rm eff} \lesssim 0.5$ (Rodriguez et al. 2019). The rates of multiple BH mergers decrease significantly for spinning BHs, as their merger experiences a recoil kick of magnitude comparable or larger to the escape speed of the cluster (Rodriguez et al. 2019). On the other hand, a massive stellar field triple is less likely to be disrupted during the inner BBH merger (Section 2). A pile-up of GW sources in the mass gap with $\chi_{\rm eff} \gg 0$ could be an indicative of isolated triple origin. Additionally, systems in which both BH have masses above the mass gap and $\chi_{\rm eff} < 0$ should be seriously considered of cluster origin.

Multiple stellar systems have also been associated to BBH mergers. Standard evolving hierarchical triples of field or cluster origin can lead to an inner BBH merger by perturbations of the third companion (Fragione & Kocsis 2020; Martinez et al. 2020). Standard evolving quadruple systems have also been suggested as progenitors of BBH mergers. Some of them can be composed of two BBH binaries, where recoil kick of the merger remnant of one BBH triggers the interaction with the other BBH, likely exchanging a component and eventually leading to a BBH merger (Fragione

et al. 2020). Others can be hierarchical quadruples where the Lidov-Kozai effect assists the sequential merger of the two inner binaries (Safarzadeh et al. 2020).

Alternatively, some BBHs orbiting around galactic nuclei can experience Lidov-Kozai perturbations from the central super-massive black hole, increasing the BBH merger rate (Hoang et al. 2018).

4.5. *Intermediate mass-ratio inspirals*

Sequential mergers with $M_{\rm BBH,in} > 100$ M$_\odot$ and $M_{\rm BH,3} < 43$ M$_\odot$, which correspond to the red and yellow region above the mass gap in Figures 1 and 2, are intermediate mass-ratio inspirals (IMRIs) and can be degenerate with those of binary origin (Appendix). BHs with $M_{\rm BH} \gtrsim 100$ M$_\odot$ are usually associated with clusters (see Miller & Colbert 2004, for a review) but can also be formed by single massive stars (Heger et al. 2003). IMRIs have not yet been detected, but the merger product of GW190521is the first detected intermediate-mass BH (Abbott et al. 2020a).

For our assumptions we expect $\chi_{\rm eff} = 0$ for IMRIs of binary origin, and therefore $\chi_{\rm eff} \gg 0$ is a strong indicative of sequential merger origin. IMRIs in the yellow region have $0.5 \lesssim \chi_{\rm eff} \lesssim 0.68$ but IMRIs in the red region have $0 \lesssim \chi_{\rm eff} \lesssim 0.1$ (Figures 1, 2, 4 and Table 1).

4.6. *Rate of sequential mergers*

At redshift $z = 0$, Riley et al. (2020) predicts a BBH merger rate of 50 Gpc^{-3} yr^{-1}, which we use to estimate a sequential merger rate $\mathcal{R} < 3$ Gpc^{-3} yr^{-1} from field triples (Appendix), similar to the estimated rate from hierarchical triples in clusters (Martinez et al. 2020) and in the field (Antonini et al. 2017).

For sequential mergers, the inner compact BBH is likely a fast merger ($\lesssim 100$ Myr) while the wide outer orbit merges in longer timescales ($\sim$Gyrs, Figure 4). This hierarchical nature leads to a cutoff in the delay time distribution at early times and a possible pile up at higher redshifts, which can be probed with third generation GW detectors (Abbott et al. 2017). It is further supported by the fact that lower metallicity environments are believed to dominate at higher redshifts.

5. CONCLUSIONS

We investigated configurations of isolated massive stellar triples that lead to sequential BBH mergers. We find that triples with CHE inner binaries are good candidates for sequential mergers. Our model predicts that GW sources with one BH in the mass gap and $\chi_{\rm eff} > 0.1$, can be of sequential merger origin. We highlight two classes of triples that lead to BBHs in the mass gap. The first one has a tertiary BH above the mass gap and $0.1 \lesssim \chi_{\rm eff} \lesssim 0.27$ (see red sub-region A in Figure 2 and Figure 4). The second one has a tertiary BH below the mass gap and $0.38 \lesssim \chi_{\rm eff} \lesssim 0.58$ (see blue sub-region B in Figure 2 and Figure 4). We suggest GW170729 is of triple origin and belongs to the second class. The masses and spins of mass gap event GW190521 are inconsistent with our model, which further supports a cluster origin.

From a broader point of view, we outlined a new outcome of the evolution of massive stellar triples from a proof-of-principle study. To improve upon the predictions made here, several processes should be considered; the effects of the uncertain initial orbital configurations of stellar triples, which may also lead to non-negligible three-body dynamical effects, the non-trivial problem of mass transfer in triples, GW recoil kicks from the inner BBH merger, and their combined effects on population statistics. Higher-order multiplicity in massive stars is crucial to understanding the most energetic astronomical phenomena in the Universe.

The authors thank David R. Aguilera-Dena, Chris Belczynski, Giacomo Fragione, Ryosuke Hirai, Ilya Mandel, Chris Moore, Ataru Tanikawa, and Team COMPAS for useful discussions and suggestions. We thank Teresa Rebagliato for the graphic representation of the formation channels. A.V-G. and E.R-R. acknowledge funding support by the Danish National Research Foundation (DNRF132). E.R-R. is also supported by the Heising-Simons Foundation and NSF (AST-1911206 and AST-1852393). S.T. acknowledges support from the Netherlands Research Council NWO (VENI 639.041.645 grants). N.W.C.L. gratefully acknowledges support from the Chilean government via Fondecyt Iniciación Grant #11180005. C.-J.H. acknowledge support of the National Science Foundation, and the LIGO Laboratory. LIGO was constructed by the California Institute of Technology and Massachusetts Institute of Technology with funding from the National Science Foundation and operates under cooperative agreement PHY-1764464.

Software: COMPAS v02.11.04 publicly available at GitHub via TeamCOMPAS/COMPAS. Scripts used for this study available in GitHub via avigna/sequential-mergers.

REFERENCES

Abbott, B. P., Abbott, R., Abbott, T. D., et al. 2017, Classical and Quantum Gravity, 34, 044001

—. 2019, Physical Review X, 9, 031040

Abbott, R., Abbott, T. D., Abraham, S., et al. 2020a, Phys. Rev. Lett., 125, 101102.

—. 2020b, The Astrophysical Journal, 900, L13.

Abbott, R., Abbott, T. D., Abraham, S., et al. 2020, ApJL, 896, L44

Abt, H. A. 1983, Annual Review of Astronomy and Astrophysics, 21, 343.

Aguilera-Dena, D. R., Langer, N., Moriya, T. J., & Schootemeijer, A. 2018, ApJ, 858, 115

Antonini, F., Toonen, S., & Hamers, A. S. 2017, ApJ, 841, 77

Astropy Collaboration, Robitaille, T. P., Tollerud, E. J., et al. 2013, A&A, 558, A33

Astropy Collaboration, Price-Whelan, A. M., SipHocz, B. M., et al. 2018, aj, 156, 123

Batta, A., & Ramirez-Ruiz, E. 2019, arXiv e-prints, arXiv:1904.04835.

Belczynski, K., Kalogera, V., & Bulik, T. 2002, ApJ, 572, 407

Belczynski, K. 2020, arXiv e-prints, arXiv:2009.13526.

Blaauw, A. 1961, BAN, 15, 265

Boyle, L., Kesden, M., & Nissanke, S. 2008, PhRvL, 100, 151101

Chatziioannou, K., Cotesta, R., Ghonge, S., et al. 2019, PhRvD, 100, 104015

Costa, G., Bressan, A., Mapelli, M., et al. 2020, arXiv e-prints, arXiv:2010.02242.

de Mink, S. E., & Mandel, I. 2016, MNRAS, 460, 3545

de Vries, N., Portegies Zwart, S., & Figueira, J. 2014, MNRAS, 438, 1909

du Buisson, L., Marchant, P., Podsiadlowski, P., et al. 2020, MNRAS, 499, 5941

Farmer, R., Renzo, M., de Mink, S. E., Marchant, P., & Justham, S. 2019, ApJ, 887, 53

Farmer, R., Renzo, M., de Mink, S. E., Fishbach, M., & Justham, S. 2020, ApJL, 902, L36

Farrell, E. J., Groh, J. H., Hirschi, R., et al. 2020, arXiv e-prints, arXiv:2009.06585.

Fishbach, M., & Holz, D. E. 2020, ApJL, 904, L26

Fragione, G., & Kocsis, B. 2020, MNRAS, 493, 3920

Fragione, G., Loeb, A., & Rasio, F. A. 2020, ApJL, 895, L15

Fryer, C. L., Belczynski, K., Wiktorowicz, G., et al. 2012, ApJ, 749, 91

Fuller, J., & Ma, L. 2019, ApJL, 881, L1

González, J. A., Sperhake, U., Brügmann, B., Hannam, M., & Husa, S. 2007, PhRvL, 98, 091101

Haster, C.-J., Antonini, F., Kalogera, V., & Mand el, I. 2016a, ApJ, 832, 192

Haster, C.-J., Wang, Z., Berry, C. P. L., et al. 2016b, MNRAS, 457, 4499

He, M. Y., & Petrovich, C. 2018, MNRAS, 474, 20

Heger, A., Fryer, C. L., Woosley, S. E., Langer, N., & Hartmann, D. H. 2003, ApJ, 591, 288

Heger, A., & Woosley, S. E. 2002, ApJ, 567, 532

Hoang, B.-M., Naoz, S., Kocsis, B., Rasio, F. A., & Dosopoulou, F. 2018, ApJ, 856, 140

Hurley, J. R., Pols, O. R., & Tout, C. A. 2000, Mon. Not. Roy. Astron. Soc., 315, 543

Iben, Icko, J., & Tutukov, A. V. 1999, ApJ, 511, 324

Inayoshi, K., Hirai, R., Kinugawa, T., & Hotokezaka, K. 2017, MNRAS, 468, 5020

Jiménez-Forteza, X., Keitel, D., Husa, S., et al. 2017, PhRvD, 95, 064024

Kimball, C., Talbot, C., Berry, C. P. L., et al. 2020, ApJ, 900, 177

Langer, N. 2012, ARA&A, 50, 107

Leigh, N. W. C., & Geller, A. M. 2013, MNRAS, 432, 2474

Leigh, N. W. C., Lützgendorf, N., Geller, A. M., et al. 2014, MNRAS, 444, 29

Leigh, N. W. C., Toonen, S., Portegies Zwart, S. F., & Perna, R. 2020, MNRAS, 496, 1819

LIGO Scientific Collaboration. 2018, LIGO Algorithm Library - LALSuite, free software (GPL), , , doi:10.7935/GT1W-FZ16

Lousto, C. O., Campanelli, M., Zlochower, Y., & Nakano, H. 2010, Classical and Quantum Gravity, 27, 114006

Maeder, A. 1987, A&A, 178, 159

Mangiagli, A., Bonetti, M., Sesana, A., & Colpi, M. 2019, ApJL, 883, L27

Marchant, P., Langer, N., Podsiadlowski, P., Tauris, T. M., & Moriya, T. J. 2016, A&A, 588, A50

Mardling, R. A., & Aarseth, S. J. 2001, MNRAS, 321, 398

Marigo, P., Girardi, L., Chiosi, C., & Wood, P. R. 2001, A&A, 371, 152

Martinez, M. A. S., Fragione, G., Kremer, K., et al. 2020, ApJ, 903, 67

Miller, M. C., & Colbert, E. J. M. 2004, International Journal of Modern Physics D, 13, 1

Moe, M., & Di Stefano, R. 2017, ApJS, 230, 15

Müller, B., Heger, A., Liptai, D., & Cameron, J. B. 2016, MNRAS, 460, 742

Naoz, S. 2016, ARA&A, 54, 441

Neijssel, C. J., Vigna-Gómez, A., Stevenson, S., et al. 2019, MNRAS, 490, 3740

Öpik, E. 1924, Publications of the Tartu Astrofizica Observatory, 25

Peters, P. C. 1964, Physical Review, 136, B1224

Planck Collaboration, Ade, P. A. R., Aghanim, N., et al. 2016, A&A, 594, A13

Podsiadlowski, P., Joss, P. C., & Hsu, J. J. L. 1992, ApJ, 391, 246

Portegies Zwart, S. F., & McMillan, S. L. W. 2000, ApJL, 528, L17

Riley, J., Mandel, I., Marchant, P., et al. 2020, arXiv e-prints, arXiv:2010.00002

Rodriguez, C. L., Zevin, M., Amaro-Seoane, P., et al. 2019, PhRvD, 100, 043027

Safarzadeh, M., Hamers, A. S., Loeb, A., & Berger, E. 2020, ApJL, 888, L3

Samsing, J., & Hotokezaka, K. 2020, arXiv e-prints, arXiv:2006.09744

Sana, H., de Mink, S. E., de Koter, A., et al. 2012, Science, 337, 444

Sana, H., Le Bouquin, J.-B., Lacour, S., et al. 2014, The Astrophysical Journal Supplement Series, 215, 15.

Shenar, T., Gilkis, A., Vink, J. S., Sana, H., & Sand er, A. A. C. 2020, A&A, 634, A79

Sigurdsson, S., & Hernquist, L. 1993, Nature, 364, 423

Stevenson, S., Vigna-Gómez, A., Mandel, I., et al. 2017, Nature Communications, 8, 14906

Stevenson, S., Sampson, M., Powell, J., et al. 2019, ApJ, 882, 121

Tanikawa, A., Kinugawa, T., Yoshida, T., Hijikawa, K., & Umeda, H. 2020, arXiv e-prints, arXiv:2010.07616.

Tokovinin, A. 2017, ApJ, 844, 103

Toonen, S., Hamers, A., & Portegies Zwart, S. 2016, Computational Astrophysics and Cosmology, 3, 6

Toonen, S., Portegies Zwart, S., Hamers, A. S., & Bandopadhyay, D. 2020, A&A, 640, A16

van Son, L. A. C., De Mink, S. E., Broekgaarden, F. S., et al. 2020, ApJ, 897, 100

Vigna-Gómez, A., Neijssel, C. J., Stevenson, S., et al. 2018, MNRAS, 481, 4009

Vigna-Gómez, A., Justham, S., Mandel, I., de Mink, S. E., & Podsiadlowski, P. 2019, ApJL, 876, L29

APPENDIX

A. RAPID POPULATION SYNTHESIS

We use the publicly available data from Riley et al. (2020) for synthetic BBH formation and merger rates. That study made use of the COMPAS rapid population synthesis code (Stevenson et al. 2017; Vigna-Gómez et al. 2018; Neijssel et al. 2019), which is freely available at http://github.com/TeamCOMPAS/COMPAS. The version of COMPAS used for these simulations was v02.11.01a, built specifically for Riley et al. (2020); functionality in this release was integrated into the public COMPAS code base in v02.11.04.

Riley et al. (2020) performs, for the first time, simultaneous population synthesis of CHE and standard evolving binaries. We use the orbital distributions of BBH mergers from that study as an educated guess for the properties of the inner BBH in the sequential merger scenario. While this works well as a first approach, the initial conditions from Riley et al. (2020) are based on birth distributions from observations of isolated massive binaries (Sana et al. 2012). Riley et al. (2020) simulates binaries with metallicities $-4 \leq \log_{10} Z \leq -1.825$. As there are no binary evolution models available at zero-metallicity Pop III stars, all of our quantitative results from compact binaries come exclusively from CHE binaries.

The most relevant conclusions drawn from this data concerning sequential mergers are:

- There are, overall, $\sim 4\times$ more merging BBH from standard evolving than from CHE binaries. The local merger rate ($z = 0$), which accounts for star formation history and galaxy mass-metallicity dependence, are 50 and 20 Gpc^{-3} yr^{-1} for isolated binaries and the subset of CHE binaries respectively. For CHE binaries we include massive over-contact binaries. A massive over-contact binary can fill its inner Lagrangian point during the main sequence as long as the outer Lagrangian point is not filled (Marchant et al. 2016).

- The yield of merging BBH from CHE binaries is roughly constant below $\log_{10} Z/\mathrm{Z}_\odot \lesssim -0.5$ (c.f. Figure 6 of Riley et al. 2020), with $\mathrm{Z}_\odot = 0.0142$. Low-metallicity CHE stars are more compact than high-metallicity ones; they also experience less mass loss and orbital widening through stellar winds.

- The maximum pre-merger total mass of BBHs for both CHE and standard evolving binaries is $M_{\mathrm{BH},1} + M_{\mathrm{BH},2} \approx 79\ \mathrm{M}_\odot$.

- In this COMPAS data set, there are no BBH above the mass gap. This holds even when including stars with initial masses up to 150 $\mathrm{M}_\odot$, for which the adopted stellar evolution models from Hurley et al. (2000) are extrapolated to stars above 50 $\mathrm{M}_\odot$. However, we consider there is a possibility of BBHs above the mass gap in Nature. They could come from standard evolving stars (e.g. Mangiagli et al. 2019) or CHE binaries (e.g. Marchant et al. 2016; du Buisson et al. 2020).

- We use the *delayed* supernova mechanism prescription from Fryer et al. (2012) to determine the remnant mass and natal kick distributions. This prescription predicts complete fallback for BH progenitors with carbon-oxygen core masses above 11 $\mathrm{M}_\odot$. In our population, more than half of standard evolving stars and all CHE stars leading to BBHs have masses above this threshold. Complete fallback has two implications. The first one is that the final baryonic mass of the remnant is the same as the pre-supernova mass (Equations 19 and 20 from Fryer et al. 2012) modulo neutrino emission. The second one is that there are no natal kicks for heavy BHs (Equation 21 of Fryer et al. 2012).

We emphasize that a full population synthesis of massive stellar triples will help us understand better the evolution of sequential mergers, their delay time distribution and constrain their rates. We hope future software developments and observations will make this sort of study possible in the near future.

B. RADIATED MASS DURING BBH MERGERS

For a BBH, f_{rad} is the amount of energy radiated away in the form of gravitational waves during the coalescence, expressed as a fraction of the total mass of the BBH. While the magnitude of f_{rad} is independent of the BBH total mass, it does depend on the binary mass ratio $q_{\mathrm{in}} = M_{\mathrm{BH},2}/M_{\mathrm{BH},1}$ (with $M_{\mathrm{BH},1} \geq M_{\mathrm{BH},2}$) and the BH spin configuration. More specifically, it depends on $\chi_{1,2}^{L||} \equiv \chi_{1,2}\cos(\theta_{1,2})$, with $0 \leq \chi_{1,2} \leq 1$ being the BH spin magnitude

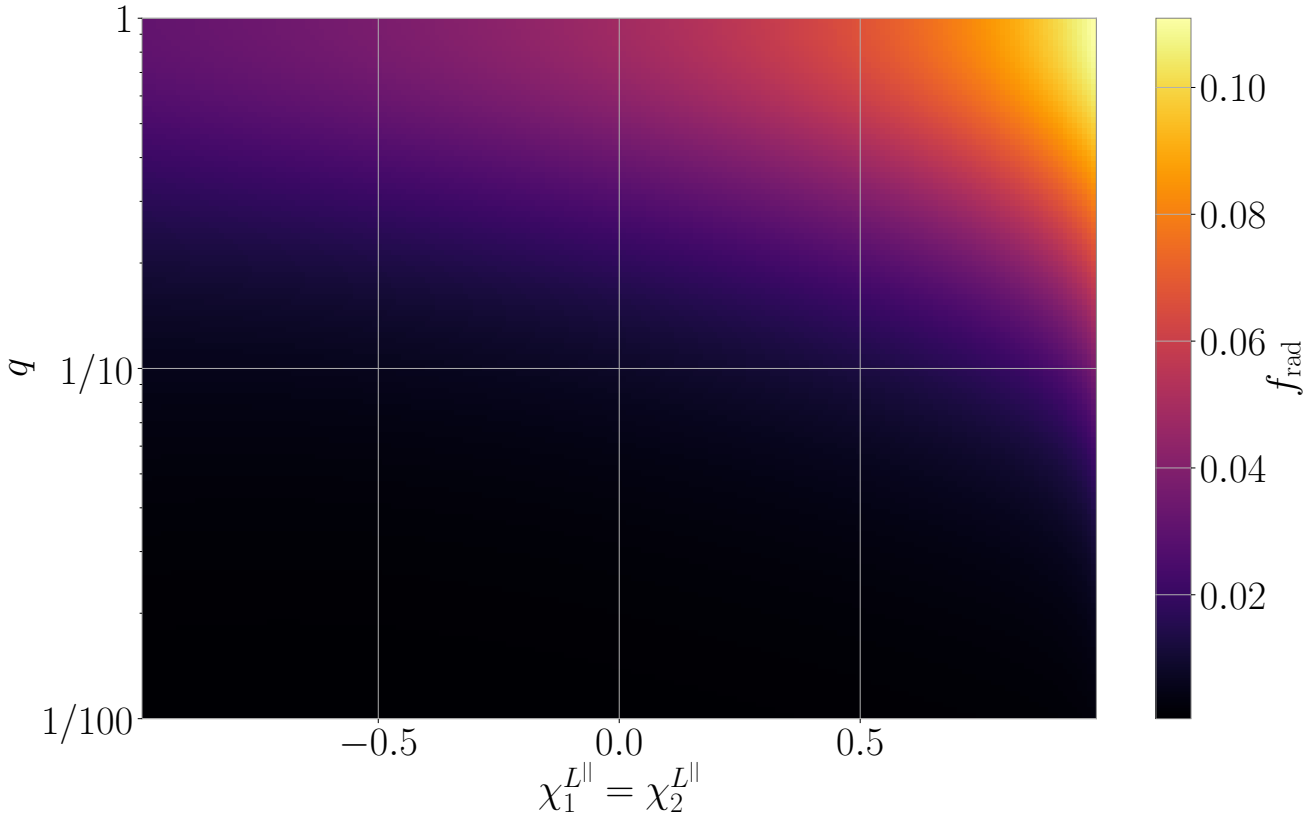

Figure 5. Radiated mass fraction, $f_{\rm rad}$, from a BBH merger. For simplicity, we present the case for equal spins aligned with the orbital angular momentum vector $\hat{L}_{\rm N}$. In the Letter we focus on the non-rotating scenario with $\chi_{1,2}^{L||} = 0$. We use this to estimate the GW Blaauw kick of the inner BBH merger in Section 2.

and $\theta_{1,2}$ the zenith angle between the spin and orbital angular momenta at the time of merger for each BH. $f_{\rm rad}$ is typically approximated by making use of fitting formulae that are based on numerical relativity simulations of BBHs.

In this study, we use the prescription from Equation 28 of Jiménez-Forteza et al. (2017) as implemented in LALSuite (LIGO Scientific Collaboration 2018) and show $f_{\rm rad}$ for a selection of BH spins and mass ratios in Figure 5. For simplicity, and following our assumptions, we have restricted the figure to binaries with equal $\chi_{1,2}^{L||}$ values. We use this prescription to estimate the final masses from both the inner BBH merger (Figure 1 and 2) and from sequential mergers.

C. REDSHIFT ESTIMATE

In order to test the validity of the sequential merger scenario for Abbott et al. (2019), we focus on the expected delay times for our scenario. The delay time is the time it takes a system to evolve from the zero-age main-sequence to the sequential BBH merger, and follows from our models. We will convert it into a redshift in the following way. We use `astropy's cosmology` module to convert between redshift and lookback time using `astropy's lookback_time` (Astropy Collaboration et al. 2013, 2018). We assume a flat ΛCDM cosmology with $H_0 = 67.90$ km s^{-1} Mpc^{-1} and $\Omega_{\rm m} = 0.3065$ following Planck Collaboration et al. 2016. With this setup, for a delay time of ~ 5.1 Gyr, we estimate a redshift $z \approx 0.49$.

D. INTERMEDIATE MASS RATIO INSPIRALS

In Figure 2 we mark the region of sequential mergers with masses $M \geq 124$ M$_\odot$ and mass ratios $q < 0.2$ as being IMRIs. This type of systems is degenerate with IMRIs of binary origin. IMRIs have primary masses of e.g., $M_{\rm BH,1} \geq 100$ M$_\odot$ and mass ratios of e.g., $q < 0.1$ (see, e.g., Haster et al. 2016a,b). In Section 4.5 we briefly discuss that they are usually associated to cluster origin, but we do not rule out isolated origin. In Table 1 we present the properties of IMRIs from red sub-region A and yellow sub-region C.

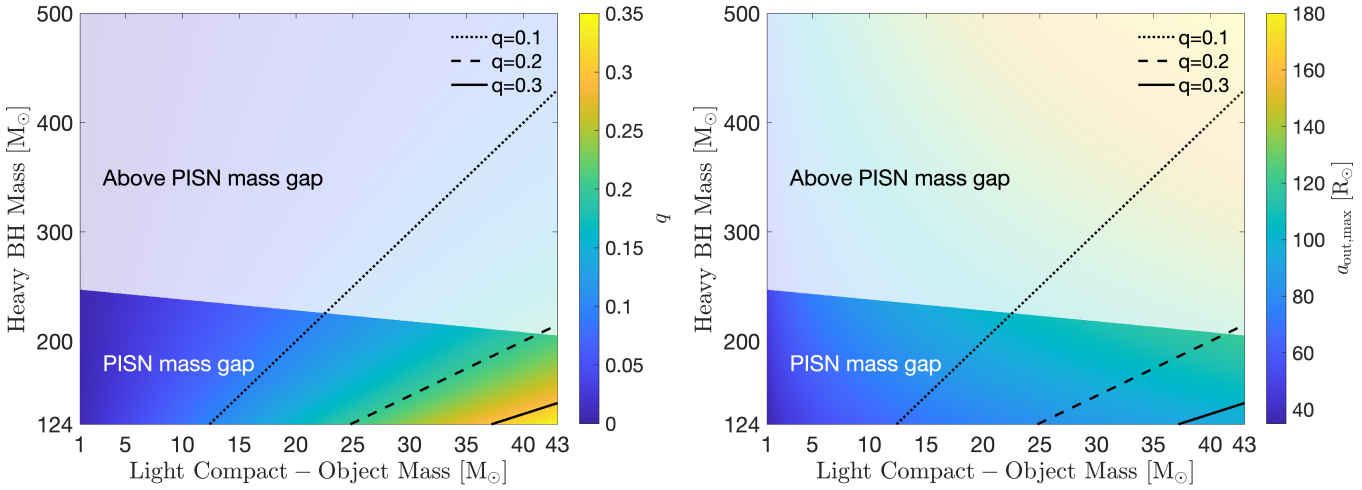

Figure 6. IMRI systems can populate the mass gap as binaries in the total mass parameter space, but if their component masses are properly resolved they can be excluded. The transparency shows the region outside the mass gap. This plot is similar to the red region from Figure 1 in the limit where $M_{\rm BH,2} \ll M_{\rm BH,1}$.

In this Appendix we briefly expand our analysis of sequential mergers leading to systems that are degenerate in mass with IMRIs. Figure 6 considers double compact objects with primary masses $124 \leq M_{\rm BH,1}/{\rm M}_\odot \leq 500$ and light compact-object masses $1 \leq M_{\rm light}/{\rm M}_\odot \leq 43$. In this case, light compact-objects include both neutron stars and black holes. It is not dependent of the maximum mass of neutron stars nor the existence or absence of a mass gap between neutron stars and black holes. These limits constrain the mass ratio to $0 \lesssim q \lesssim 0.35$. To date GW190814 is the gravitational-wave source with the most extreme mass ratio of $q = M_{\rm light}/M_{\rm BH,1} \approx 2.6/23 \approx 0.11$ (Abbott et al. 2020). However, the individual masses of GW190814 are well below those of typical IMRIs.

For an IMRI the inference of the effective spin might not be enough to classify their origin. For a sequential merger, if the tertiary is the most massive component then the effective spin is dominated by this massive non-rotating BH, i.e. $\chi_{\rm eff} \approx 0$. This value would be similar to that of a non-rotating binary. On the other hand, if the tertiary is the least massive component, that effective spin is $\chi_{\rm eff} \approx 0.7$. This is visually summarized in Figure 4 and quantitatively in Table 1.

More detailed studies of the spin properties of BBH mergers from isolated binary, isolated triple and cluster origin would help in the classification of future detections of IMRIs. Additionally, population studies might be helpful in constraining the merger rates from different formation channels.

E. SEQUENTIAL MERGERS RATE ESTIMATE

In order to give an upper limit in the local ($z = 0$) rate of sequential mergers ($\mathcal{R}$) we make a simple estimate in the form

$$\mathcal{R} = \mathcal{R}_{\rm BBH,in} \times (f_{\rm triple}/f_{\rm binary}) \times f_{\rm separation}. \tag{E1}$$

We estimate the BBH merger rate $\mathcal{R}_{\rm BBH,in} = 50$ Gpc^{-3} yr^{-1} based on the isolated binary evolution calculations of Riley et al. (2020), which accounts for both compact and standard evolving stars. This optimistic rate includes sequential mergers with total mass below the mass gap. Riley et al. (2020) assumes that a fraction $f_{\rm binary} = 0.7$ of massive star systems are binaries. The factor $f_{\rm triple} = 0.35$ describes the fraction of massive star systems that are stellar triples (Moe & Di Stefano 2017).

The factor $f_{\rm separation}$ accounts for the fraction of systems in which the outer orbital can merge within a Hubble time due to gravitational-wave emission. To estimate $f_{\rm separation}$ we assume the log of the outer birth orbital separation is distributed uniformly $p(a_{\rm out}) \propto a_{\rm out}^{-1}$ (Öpik 1924; Abt 1983). We then estimate the fraction of systems of interest in the form:

$$f_{\rm separation} = \frac{\int_{a_{\rm out-SM,min}}^{a_{\rm out-SM,max}} a^{-1} da}{\int_{a_{\rm out,min}}^{a_{\rm out,max}} a^{-1} da} = \frac{\int_{35\ {\rm R}_\odot}^{135\ {\rm R}_\odot} a^{-1} da}{\int_{28\ {\rm R}_\odot}^{2\times10^6\ {\rm R}_\odot} a^{-1} da} \approx 0.12, \tag{E2}$$

where $a_{\rm out}$ is the outer separation of stable triples, and $a_{\rm out-SM}$ is the outer separation of potential sequential mergers. The lower limit on $a_{\rm out}$ is given by the smallest value for a stable triple with an inner binary separation $a_{\rm in} \approx 10$ R$_\odot$, $(a_{\rm out}/a_{\rm in})_{\rm crit} = 2.8$, and therefore $a_{\rm out,min} = 28$ R$_\odot$. The maximum outer separation at birth we consider is $a_{\rm out,max} \approx 10^4$ AU $\approx 2 \times 10^6$ R$_\odot$ (Moe & Di Stefano 2017). For the outer separation of potential sequential mergers, following the results of Table 1 as shown in top right panel of Figure 4, the limits are $35 \lesssim a_{\rm out-SM}/R_\odot \lesssim 135$. These limits in $a_{\rm out-SM}$ assume that the separation does not drastically change from the zero-age main sequence until the inner BBH merger. For some triples, this assumption will not necessarily hold (Section 4). For when it holds, we expect the distribution of merger times to be $p(t) \propto t^{-1}$, as expected from gravitational-wave dominated binaries with a flat-in-the-log distribution at BBH formation. This assumption also neglects initially wider tertiary stars which are stripped and become potential sequential mergers (Section 3.3.1), which would increase the values of $a_{\rm out-SM,max}$, $f_{\rm separation}$ and ultimately the rate. The assumption of different orbital initial distributions would naturally also affect the rates. We choose these assumptions for an order-of-magnitude estimate and leave a more thorough analysis of the orbital parameter space and the distribution of merger times for a future study.

After substituting all of the estimated parameters in Equation E1, we constrains the upper limit to $\mathcal{R} < 3$ Gpc^{-3} yr^{-1} for sequential mergers.

F. MORE DETAILS ON THE EVOLUTION OF GW170729

As a proof of concept of the evolution towards sequential mergers, we have simulated the evolution of the proposed progenitor of GW170729 with two independent codes: the rapid binary population synthesis code COMPAS and the triple evolution code `TRES` (Toonen et al. 2016, 2020). We use these codes to model the evolution from the zero-age main sequence to the inner BBH merger.

We use COMPAS as described in Appendix A to explore a binary system that is representative of the CHE inner binary for a GW170729-like system. We follow the evolution from the zero-age main sequence until BBH formation. This system consists initially of a circular CHE binary with $M_1 = M_2 = 29$ M$_\odot$, $R_1 = R_2 = 4.8$ R$_\odot$ and $a = 10.2$ R$_\odot$. The separation, masses, and radial time evolution is shown in Figure 7. CHE are expected to contract throughout their lifetimes (see, e.g., Aguilera-Dena et al. 2018); however, the current implementation of them in COMPAS assumes a fixed radius during the main sequence. The low metallicity results in negligible mass loss and the orbit barely changes throughout the full evolution. There are two milestones in the evolution. The first one is the evolution after hydrogen depletion (≈ 6.8 Myr), when each component becomes a 1.8 R$_\odot$ naked helium star. The final one is the failed supernova (≈ 7.1 Myr), which reduces the mass by 10% (Section A), increases the separation to $a = 11.6$ R$_\odot$ and the eccentricity to $e = 0.07$. This BBH merges in ≈ 76 Myr (Peters 1964).

Additionally, we modified the triple evolution code `TRES` (Toonen et al. 2016, 2020) to model the evolution, from the zero-age main sequence until the BBH coalescence of a compact inner binary of a triple system. The inner binary consists of CHE system with $M_1 = M_2 = 29$ M$_\odot$, $R_1 = R_2 = 4.8$ R$_\odot$, $a_{\rm in} = 10.3$ R$_\odot$ and $e_{\rm in} = 10^{-5}$ (this eccentricity is the lower limit allowed in `TRES` for numerical reasons). Similarly to COMPAS, the radial evolution of all compact stars throughout the main sequence is kept constant. The tertiary is also assumed to be a compact star with $M_3 = 33$ M$_\odot$, and $R_3 = 5.2$ R$_\odot$ in an orbit of $a_{\rm out} = 45$ R$_\odot$, $e_{\rm out} = 10^{-5}$, and relative inclination $i = 0.0$. The complete orbital evolution is shown in Figure 8. There are four milestones in the evolution of this triple system. The first one is the formation of an outer 33.4 M$_\odot$ BH at ≈ 6 Myr. The second one is the evolution after hydrogen depletion (≈ 6.8 Myr), when each component of the inner binary becomes a 1.8 R$_\odot$ naked helium star. The third one is the supernovae (≈ 7.1 Myr) of the stars in the inner binary which result in two BHs of $M_{\rm BH,1} = M_{\rm BH,2} = 28.5$ M$_\odot$, $a_{\rm in} = 10.4$ R$_\odot$, $e_{\rm in} \approx 2 \times 10^{-4}$, $e_{\rm out} \approx 0.8 \times 10^{-4}$ and $i \approx 10^{-5}$. The final milestone is the gravitational-wave evolution from the inner binary; the inner BBH merges at ≈ 46 Myr. The triple remains approximately circular and co-planar throughout the evolution, validating our assumptions at the moment of triple BH formation and throughout the sequential merger.

In summary, we used two independent codes to test the validity of our assumptions in Section 2. With COMPAS we validate the compact inner binary evolution. We use `TRES` to do a dynamical calculation to corroborate that, following our initial conditions, there are no major orbital changes which would modify our assumptions during both BBH mergers. Finally, we show that our numerical results are consistent with our semi-analytical formalism.

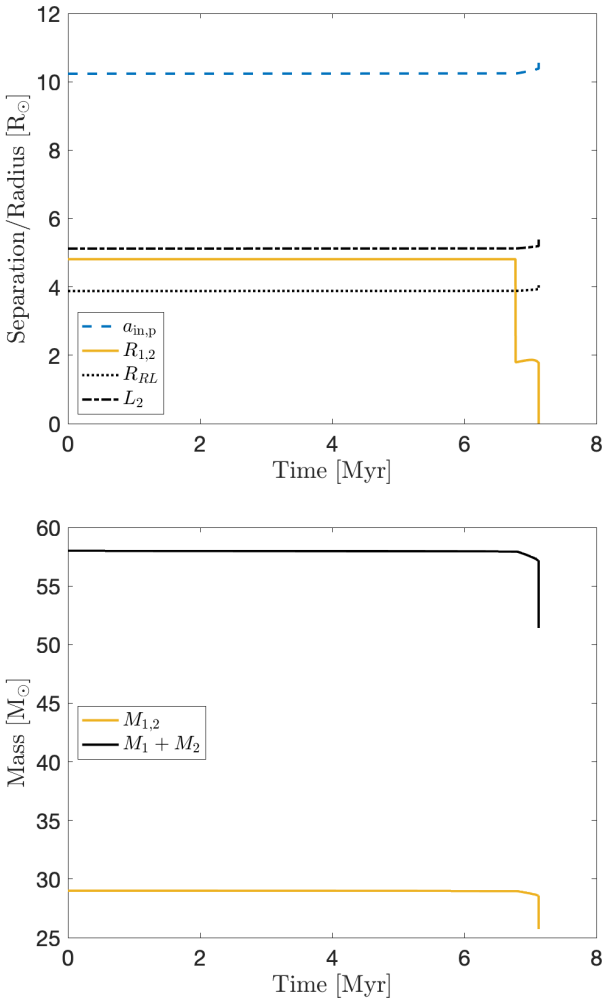

Figure 7. COMPAS time evolution, from zero-age main sequence to BBH formation, of a CHE binary at $Z = 10^{-4}$. Top: separation (dashed blue), radius (solid yellow), Roche lobe (black dotted) and second Lagrangian point (black dot-dashed). Bottom: individual masses (solid yellow) and total mass (solid black).

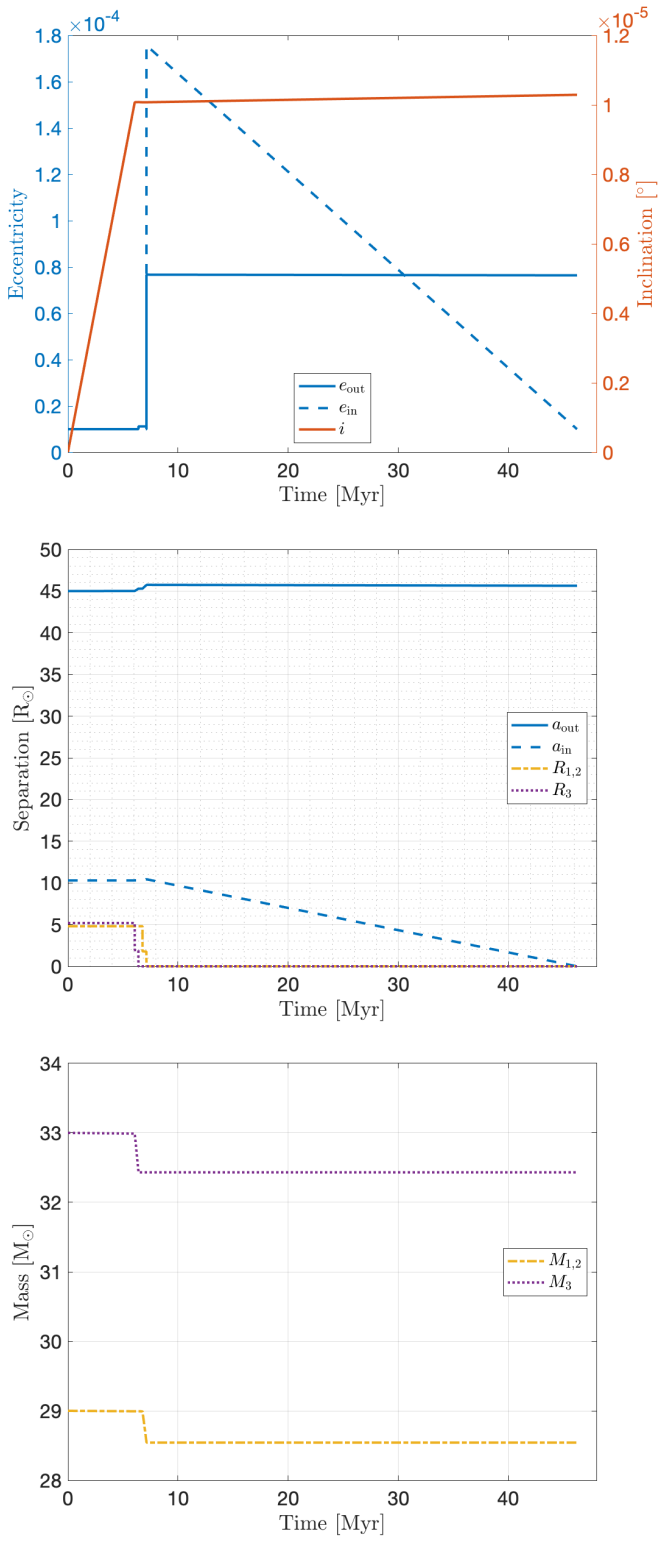

Figure 8. TRES time evolution, from zero-age main sequence to inner BBH merger, of a triple leading to a GW170729-like system (Section 3.4). Top: outer eccentricity (solid blue), inner eccentricity (dashed blue) and relative inclination (solid orange). Middle: outer separation (solid blue), inner separation (dashed blue), radius of the stars in the inner binary (dot-dashed yellow) and radius of the tertiary star (dotted purple). Bottom: mass of the stars in the inner binary (dot-dashed yellow) and mass of the tertiary star (dotted purple).